POLITECNICO DI TORINO
Repository ISTITUZIONALE

Bonding strength of glass-ceramic trabecular-like coatings to ceramic substrates for prosthetic applications

Original
Bonding strength of glass-ceramic trabecular-like coatings to ceramic substrates for prosthetic applications / Chen, Q., Baino, F., Pugno, N.M., VITALE BROVARONE, C.. - In: MATERIALS SCIENCE AND ENGINEERING. C, BIOMIMETIC MATERIALS, SENSORS AND SYSTEMS. - ISSN 0928-4931. - ELETTRONICO. - 33:(2013), pp. 1530-1538. [10.1016/j.msec.2012.12.058]

Availability:
This version is available at: 11583/2505274 since: 2016-11-19T19:11:01Z

Publisher:
Elsevier

Published
DOI:10.1016/j.msec.2012.12.058

Terms of use:

This article is made available under terms and conditions as specified in the corresponding bibliographic description in the repository

Publisher copyright

(Article begins on next page)

08 October 2026

Bonding strength of glass-ceramic trabecular-like coatings to ceramic substrates for prosthetic applications

Qiang Chen[a,b], Francesco Baino[c,]*, Nicola M. Pugno[b], Chiara Vitale-Brovarone[c]

This is the author post-print version of an article published on *Materials Science and Engineering: C*, Vol. 33, pp. *1530-1538, 2013* (ISSN *0928-4931*).
The final publication is available at
http://dx.doi.org/10.1016/j.msec.2012.12.058
This version does not contain journal formatting and may contain minor changes with respect to the published edition.
The present version is accessible on PORTO, the Open Access Repository of the Politecnico of Torino, in compliance with the publisher's copyright policy.
Copyright owner: *Elsevier*.

[a] *Laboratory of Biomechanics, School of Biological Science and Medical Engineering, Southeast University, 210096, Nanjing, P. R. China.*

[b] *Laboratory of Bio-inspired Nanomechanics "Giuseppe Maria Pugno", Structural Engineering and Geotechnics Department, Politecnico di Torino, Corso Duca degli Abruzzi 24, 10129 Torino, Italy.*

[c] *Institute of Materials Physics and Engineering, Applied Science and Technology Department, Politecnico di Torino, Corso Duca degli Abruzzi 24, 10129 Torino, Italy.*

*Corresponding author: F. Baino

Tel.: +39 011 564 4668

Fax: +39 011 564 4699

E-mail: francesco.baino@polito.it

Abstract

A new approach based on the concepts of quantized fracture mechanics (QFM) is presented and discussed in this paper to estimate the bonding strength of trabecular-like coatings, i.e. glass-ceramic scaffolds mimicking the architecture of cancellous bone, to ceramic substrates. The innovative application of glass-derived scaffolds as trabecular-like coatings is proposed in order to enhance the osteointegration of prosthetic ceramic devices. The scaffolds, prepared by polymeric sponge replication, are joined to alumina substrates by a dense glass-ceramic coating (interlayer) and the so-obtained 3-layer constructs are investigated from micro-structural, morphological and mechanical viewpoints. In particular, the fracture strengths of three different crack propagation modes, i.e. glass-derived scaffold fracture, interface delamination or mixed fracture, are predicted in agreement with those of experimental mechanical tests. The approach proposed in this work could have interesting applications towards an ever more rational design of bone tissue engineering biomaterials and coatings, in view of the optimization of their mechanical properties for making them actually suitable for clinical applications.

Keywords: Scaffold; Glass; Coating; Quantized fracture mechanics; Osteointegration.

1. Introduction

Biological materials are renowned for their unique combination of outstanding mechanical properties and smart microstructure. For instance, cancellous bone is a highly porous natural material with excellent stiffness and strength (typically 2-12 MPa in compression [1]), and these remarkable mechanical properties are attributed to its anisotropic structure possessing optimized strength-to-density and stiffness-to-density ratios [2,3]. Such features provide interesting cues on how to develop new scaffolds to mirror Nature's efficient materials from architectural/mechanical viewpoints and to substitute natural tissue functions, which is one of the greatest challenges in modern regenerative medicine.

Architectural design of bone tissue engineering scaffolds is a complex issue because, from a structural viewpoint, two competing requirements have to be basically fulfilled: on one hand, the scaffold should exhibit a sufficient mechanical competence, i.e. strength and stiffness comparable to those of natural bone, but, on the other hand, it should allow new bone in-growth after its implantation into human body [4-6]. These requirements typically involve a porosity above 50 vol.% to allow blood vessels supply, cells migration and new tissue in-growth, as well as the presence of macropores in the 100-500 μm range [4]. These features compete with the mechanical requirements, which are further discriminated if the scaffold is resorbable, as its integrity progressively decreases over time during the contact with biological fluids [7]. Furthermore, another crucial issue concerns the scaffold ability to promote bone regeneration and angiogenesis; in this sense, bioactive glasses have a great potential and constitutes a highly valuable class of biomaterials for tissue engineering [8,9].

The choice of a proper method of fabrication plays a key role in designing scaffolds structures on the basis of the final clinical use (e.g. load-bearing needs). At present, there is a great variety of methods for scaffolds processing that lead to porous body with different structures, architectures, pore sizes and interconnections, as well as different properties *in vitro* and *in vivo*, but, at present, a "gold standard" method for scaffolding has not been defined yet [6,10,11]. Sponge replication is a promising candidate for scaffolds fabrication due to its relative easiness of application, effectiveness, versatility and low cost; it was demonstrated that, by carefully setting the processing parameters [12,13] and/or by producing pore gradient structures [14], high-strength 3-D scaffolds closely mimicking human bone architecture can be successfully obtained. Some research groups investigated in detail the porosity-strength relationship in the attempt at optimizing the architectural properties of scaffolds, ideally at a pre-processing stage. Gerhardt and Boccaccini [15] showed that linear interpolation usually provides an acceptable approximation of the negative relationship between porosity and compressive strength of bioceramic scaffolds. Baino et al. [16] proposed simple quadratic models correlating the theoretical porosity, established at the design stage, with the real pore content and compressive strength of final glass-ceramic sintered scaffolds. Hellmich and co-workers [17-19] developed micromechanical models of porous ceramics and established non-linear strength-porosity relations that were in good accordance with experimental findings.

The keen attention of the scientific community towards the potential of bioactive glass-derived scaffolds for bone tissue engineering applications has been demonstrated by the dramatically increasing number of articles published since 2000 in the field, including four comprehensive reviews only in the last couple of years [6,10,20,21].

In a recently-deposited patent [22], the authors proposed the innovative use of glass and glass-

ceramic scaffolds as bioactive trabecular-like coatings on prosthetic devices with the aim to enhance the implant osteointegration (Fig. 1). The feasibility of such an application was demonstrated and discussed in a preliminary work by Vitale-Brovarone et al. [23]; in the present work, the authors developed a mechanical model based on quantized fracture mechanics (QFM) [24-26] to describe the bonding strength at the trabecular coating (scaffold)/ceramic substrate interface.

The use of QFM for modelling the mechanical behaviour of glass-derived porous coatings represents a new approach. Linear elastic fracture mechanics (LEFM) was often used in the past to describe the mechanical behaviour of pore-free biomedical materials; for instance, Ritter et al. [27] employed LEFM to obtain lifetime predictions for bioglass-coated alumina implants. The mechanical behaviour of porous ceramic scaffolds has been more recently described either by semi-empirical approaches based on data fitting [15,16] or through complex models based on continuum micro-mechanics [17-19]. However, all these works are based on the continuum, and therefore these methods are not suitable for the strength prediction of porous biomaterials without invoking often inaccurate homogenization techniques.

Differently from the above-mentioned methods and starting from the energy approach, Pugno and co-workers [24-26] developed QFM to treat fracture in discrete materials: comparison between the theory and the experimental results on several nanosystems, including carbon nanotubes and graphene, showed a very good agreement. Considering the case of porous scaffolds, characterized by an intrinsic structural discreteness, QFM has a unique advantage over LEFM and, in general, continuum theories.

In this paper, in order to properly measure the bonding strength between trabecular coating and ceramic substrate from a quantitative viewpoint, three sets of experiments were performed and the

results were compared with QFM predictions. By the fitting between experimental data and theoretical prediction, the strain energy release rate was obtained; then, it was employed to investigate the designable bonding strength influence by two dimensionless quantities.

It is worth mentioning that previous studies [28-30] on the bonding strength of biomaterials were mainly experimental, having a "descriptive" goal, and they concluded that, in general, the bonding strength was weak. On the contrary, the present model and method could quantitatively improve our ability not only in measuring but also in "designing" the bonding strength of biomaterials, making them more suitable for clinic applications in bone tissue engineering.

2. Experimental

2.1. Samples preparation

The innovative acetabular component shown in Fig. 1, wherein the trabecular coating (scaffold) plays a key role, was studied and modelled in a simplified flat geometry. These 3-layer plane samples, hereafter referred to as "complete plane samples", were fabricated according to a processing schedule described elsewhere by Vitale-Brovarone et al. [23]. The 6-stage preparation cycle is briefly summarized in Table 1; for better reader's understanding, the stages 1-5 are also schematically depicted in Fig. 2.

Furthermore, other two kinds of samples, i.e. SCNA-derived dense coatings on alumina (Stages 1-3 and 6) and SCNA-derived scaffolds (Stages 2, 4 and 6), were prepared and mechanically tested to obtain key mechanical parameters used in the development of the QFM-based model (section 3).

2.2. Samples characterization

Wide-angle (2θ within 10-70°) X-ray diffraction (XRD) by using a X'Pert diffractometer (working conditions: 40 kV and 30 mA; camera with Bragg-Brentano geometry, Cu Kα incident radiation, incident wavelength λ = 1.5405 Å, step size Δ(2θ) = 0.02°, fixed counting time of 1 s per step) was performed on SCNA before and after treatment at 1000 °C for 3 h to detect the presence of crystalline phases nucleated during the thermal treatment.

Scanning electron microscopy (SEM, Philips 525 M) was used for morphological investigations; the samples were silver-coated and observed under an accelerating voltage of 15 kV. Cross-sections were examined after embedding the samples in epoxy resin (Epofix, Struers), cutting by a diamond wheel (Struers Accutom) and careful polishing by #600 to #4000 SiC grit paper. Compositional analyses by energy dispersive spectroscopy (EDS; EDAX Philips 9100) were also performed.

The mechanical tests were performed according to the relevant ASTM standards [31,32] by applying tensile loads (Syntech 10/D machine, MTS Corp.; cross-head speed of 1 mm min^{-1}) up to failure to the considered samples. Specifically, the tests were carried out on three kinds of samples (as anticipated in the section 2.1): (i) SCNA-derived scaffolds (experiment 1), (ii) SCNA-derived dense coatings on alumina (experiment 2) and (iii) 3-layer complete samples (SCNA-derived trabecular coating + intermediate SCNA-derived compact coating on alumina, referred to as complete samples) (experiment 3). At least three samples for each type were tested.

Before testing, each sample was glued to two loading fixtures (16-mm diameter steel cylinders) by using an epoxy resin (Araldite® AV 119, Ciba-Geigy), which is able to withstand a maximum stress

of ~40 MPa (as declared by the manufacturer). At room temperature, the adhesive was a gel; its polymerization was achieved by a low-temperature treatment in oven (130 °C for 1 h). The failure tensile stress of the samples, σ_t (MPa), was calculated as $\sigma_t = \frac{F}{A_d}$, wherein F (N) is the failure load and A_d (mm^2) is the area measured after the test.

The Young's moduli of the different biomaterials, whose assessment was necessary for the model development (section 3), were evaluated by non-destructive acoustic measurements (GrindoSonic) as suggested by other authors [18].

3. Development of the model

In order to develop the QFM-based model, the complete plane samples were considered as constituted by three components or layers (Fig. 3a), i.e. the SCNA-derived trabecular-like coating (porous scaffold, first layer), the SCNA-derived intermediate coating (non-porous coating, second layer) and the alumina substrate (compact substrate, third layer); all of them are planar and will be denoted, for purpose of simplicity, with the superscripts "1", "2" and "3", respectively. Accordingly, the superscripts "12" and "23" will identify the scaffold/intermediate coating interface and the intermediate coating/alumina substrate interface, respectively.

3.1. Basic theory

Referring to the 3-layer structure depicted in Fig. 3a, the Young's moduli of scaffold, intermediate coating and substrate are denoted by $E^{(1)}$, $E^{(2)}$ and $E^{(3)}$, and the corresponding thicknesses are $l^{(1)}$, $l^{(2)}$

and $l^{(3)}$. The force F acts on the top face "CD" of the scaffold (Fig. 3a). The top face "*CD*" is square-shaped with side length a and area A. The side length and area of the bottom face "*AB*" are assumed to be equal to $\sqrt{\alpha}a$ and αA, respectively, wherein the condition $\alpha \neq 1$ accounts for a non-constant cross-section. After crack propagation, part I was assumed to be stressed whereas parts II and III became unstressed (Fig. 3b), as suggested by a linear asymptotic matching; the final cross-sectional area is αA (Fig. 3c).

According to LEFM, the total potential energy Π of the system is expressed as:

$$\Pi = U - W \tag{1}$$

wherein U is the strain energy and W is the work done by the external force.

U and W can be deduced as follows:

$$U = \frac{1}{2}F^2\left(\frac{1}{k^{(1)}} + \frac{1}{k^{(2)}}\right) \tag{2}$$

$$W = F(\Delta l^{(1)} + \Delta l^{(2)}) = F^2\left(\frac{1}{k^{(1)}} + \frac{1}{k^{(2)}}\right) \tag{3}$$

wherein $k^{(1)}$, $k^{(2)}$ are the stiffness of the scaffold and intermediate coating before crack propagation and $\Delta l^{(1)}$, $\Delta l^{(2)}$ are the corresponding displacements.

Accordingly, by assuming the substrate to be rigid ($k^{(3)} = \infty$) due to its large Young's modulus, the total potential energy is obtained as:

$$\Pi = -\frac{1}{2}F^2\left(\frac{1}{k^{(1)}} + \frac{1}{k^{(2)}}\right) \tag{4}$$

According to QFM, crack propagation will take place when the "quantized" strain energy release rate, $G_I^{(12)}$, reaches its critical value $G_{IC}^{(12)}$ [24], i.e.:

$$G_{IC}^{(12)} = -\frac{\Delta\Pi}{\Delta A} \tag{5}$$

wherein $G_{IC}^{(12)}$ is the critical fracture toughness along the scaffold/intermediate coating interface and $\Delta\Pi$ is the variation of the total potential energy due to the cracked area increment ΔA.

For purpose of completeness, three possible failure modes (FMs), hereafter referred to as FM-1, FM-2 and FM-3 (Fig. 4), are investigated in the following sections.

3.2. FM-1: crack along the scaffold/intermediate coating interface

In FM-1 failure occurs at the interface between scaffold and intermediate coating (Fig. 4a). From the Eq. (4), the variation of the total potential energy Π can be calculated as:

$$\Delta\Pi = -\frac{1}{2}F^2\left[\left(\frac{1}{k^{(1)\prime}}-\frac{1}{k^{(1)}}\right)+\left(\frac{1}{k^{(2)\prime}}-\frac{1}{k^{(2)}}\right)\right] \tag{6}$$

wherein $k^{(1)\prime}$ and $k^{(2)\prime}$ denote, respectively, the stiffness of the scaffold and intermediate coating after crack propagation.

The compliance $1/k^{(1)}$ can be expressed as:

$$\frac{1}{k^{(1)}} = \frac{1}{E^{(1)}}\int_0^{l^{(1)}}\frac{dy}{A(y)} \tag{7}$$

wherein $A(y)$ denotes the cross-sectional area at the general level y.

Since $A(y)$ can be expressed as

$$A(y) = \left(\sqrt{\alpha}+\frac{y}{l^{(1)}}(1-\sqrt{\alpha})\right)^2 a^2 = \left(\sqrt{\alpha}+\frac{y}{l^{(1)}}(1-\sqrt{\alpha})\right)^2 A,$$

then compliance is derived as

$$\frac{1}{k^{(1)}} = \frac{1}{E^{(1)}}\int_0^{l^{(1)}}\frac{dy}{A(y)} = \frac{l^{(1)}}{E^{(1)}A\sqrt{\alpha}}.$$

Likewise, the compliance after delamination ca be calculated as:

$$\frac{1}{k^{(1)\prime}} = \frac{1}{E^{(1)}}\int_0^{l^{(1)}}\frac{dy}{A'(y)} = \frac{l^{(1)}}{E^{(1)}A\sqrt{\alpha'}} = \frac{l^{(1)}}{E^{(1)}A\sqrt{\frac{\alpha A-\Delta A}{A}}} = \frac{l^{(1)}}{E^{(1)}\sqrt{A(\alpha A-\Delta A)}} \tag{8}$$

wherein $A'(y)$ denotes the cross-sectional area at the general level y after failure.

Combining Eq.(7) with Eq.(8), it is possible to obtain the following expression:

$$\frac{1}{k^{(1)\prime}}-\frac{1}{k^{(1)}}=\frac{l^{(1)}}{E^{(1)}\sqrt{A(\alpha A-\Delta A)}}-\frac{l^{(1)}}{E^{(1)}A\sqrt{\alpha}}=\frac{l^{(1)}}{E^{(1)}A\sqrt{\alpha}}\left(\frac{1-\sqrt{1-\frac{\Delta A}{\alpha A}}}{\sqrt{1-\frac{\Delta A}{\alpha A}}}\right)=\frac{l^{(1)}}{2E^{(1)}A^{2}\alpha^{3/2}}\frac{\Delta A}{\sqrt{1-\frac{\Delta A}{\alpha A}}} \tag{9}$$

Developing the calculations for the intermediate coating, it was possible to obtain:

$$\frac{1}{k^{(2)}}=\frac{l^{(2)}}{E^{(2)}\alpha A}$$

$$\frac{1}{k^{(2)\prime}}=\frac{l^{(2)}}{E^{(2)}\left(\alpha A-\Delta A\right)}$$

$$\frac{1}{k^{(2)\prime}}-\frac{1}{k^{(2)}}=\frac{l^{(2)}}{E^{(2)}\left(\alpha A-\Delta A\right)}-\frac{l^{(2)}}{E^{(2)}\alpha A}=\frac{l^{(2)}}{E^{(2)}A^{2}\alpha^{2}}\frac{\Delta A}{\left(1-\frac{\Delta A}{\alpha A}\right)} \tag{10}$$

Then inserting Eq.(9) and Eq.(10) into Eq.(6), the following expression was obtained:

$$\Delta\Pi=-\frac{1}{2}F^{2}\left(\frac{l^{(1)}}{2E^{(1)}A^{2}\alpha^{3/2}}\frac{\Delta A}{\sqrt{1-\frac{\Delta A}{\alpha A}}}+\frac{l^{(2)}}{E^{(2)}A^{2}\alpha^{2}}\frac{\Delta A}{\left(1-\frac{\Delta A}{\alpha A}\right)}\right) \tag{11}$$

Finally, the energy release rate $G_I^{(12)}$ is obtained:

$$G_I^{(12)}=-\frac{\Delta\Pi}{\Delta A}=\left(\sigma_I^{(12)}\right)^{2}\frac{\alpha^{1/2}l^{(1)}E^{(2)}\sqrt{1-\frac{\Delta A}{\alpha A}}+2l^{(2)}E^{(1)}}{4E^{(1)}E^{(2)}\alpha^{2}(1-\frac{\Delta A}{\alpha A})} \tag{12}$$

The crack propagation will take place when $G_I^{(12)}=G_{IC}^{(12)}$ and can be stable, metastable or unstable according to the following criteria [24]:

$$\begin{cases}\dfrac{dG_I^{(12)}}{d\left(\Delta A\right)}<0, \textit{stable}\\ \dfrac{dG_I^{(12)}}{d\left(\Delta A\right)}=0, \textit{critical state}\\ \dfrac{dG_I^{(12)}}{d\left(\Delta A\right)}>0, \textit{unstable}\end{cases} \tag{13}$$

Combining Eq.(12) with Eq.(13), the following condition is obtained:

$$\frac{dG_I^{(12)}}{d(\Delta A)}=\left(\sigma_I^{(12)}\right)^{2}\frac{\alpha^{1/2}l^{(1)}E^{(2)}\sqrt{1-\frac{\Delta A}{\alpha A}}+4l^{(2)}E^{(1)}}{8E^{(1)}E^{(2)}\alpha^{3}A(1-\frac{\Delta A}{\alpha A})^{2}}>0\,,$$

from which it is possible to conclude that the crack propagation is always unstable.

Finally, the delamination strength is expressed as:

$$\sigma_{IC}^{(12)} = 2\alpha \sqrt{\frac{E^{(1)}E^{(2)}(1-\frac{\Delta A}{\alpha A})}{\alpha^{1/2} l^{(1)} E^{(2)} \sqrt{1-\frac{\Delta A}{\alpha A}} + 2 l^{(2)} E^{(1)}} G_{IC}^{(12)}} \tag{14}$$

If the condition $l^{(2)}E^{(1)} \ll l^{(1)}E^{(2)}$ is satisfied, then Eq. (14) can be simplified into:

$$\sigma_{IC}^{(12)} = 2\alpha^{\frac{3}{4}} \sqrt{\frac{E^{(1)}G_{IC}^{(12)}}{l^{(1)}}} \sqrt{1-\frac{\Delta A}{\alpha A}}$$

Due to vanishing of $\Delta A/\alpha A$, a further simplification occurs ($\sigma_{IC}^{(12)} = 2\alpha^{\frac{3}{4}}\sqrt{E^{(1)}G_{IC}^{(12)}/l^{(1)}}$) and, if $\alpha = 1$, the following expression is obtained:

$$\sigma_{IC}^{(12)} = 2\sqrt{E^{(1)}G_{IC}^{(12)}/l^{(1)}}\ .$$

3.3. FM-2: crack in the scaffold

In FM-2 failure occurs in the scaffold (Fig. 4b), as the strength of the scaffold is supposed to be lower than the bonding strength at the interface between intermediate dense coating and alumina.

According to QFM, the fracture stress is expressed as [24-26]:

$$\sigma_{IC}^{(1)} = \frac{K_{IC}^{(2)}}{\sqrt{\pi\left(a^{(1)} + \frac{\mathrm{q}}{2}\right)}} \tag{15}$$

wherein $\sigma_{IC}^{(1)}$ is the strength of the scaffold, $K_{IC}^{(2)}$ is the critical stress intensity factor of the intermediate dense coating, $2a^{(1)}$ is the crack length and q is the fracture quantum, that is expressed as:

$$\mathrm{q} = \frac{2}{\pi}\left(\frac{K_{IC}^{(2)}}{\sigma_{IC}^{(2)}}\right)^2 \tag{16}$$

wherein $\sigma_{IC}^{(2)}$ is the fracture strength of the intermediate coating.

Accordingly, the following expression was obtained:

$$\sigma_{IC}^{(1)} = K_{IC}^{(2)} \sqrt{\frac{1}{\pi\left(a^{(1)} + \frac{\mathrm{q}}{2}\right)}} = \frac{K_{IC}^{(2)}}{\sqrt{\pi \mathrm{q}/2}} \cdot \sqrt{\frac{1}{1 + a^{(1)}/\mathrm{q}}} = \frac{\sigma_{IC}^{(2)}}{\sqrt{1 + 2a^{(1)}/\mathrm{q}}} \tag{17}$$

Extending the result from a crack to an elliptical hole with half axes *a* and *b* [25] gives:

$$\sigma_{IC}^{(1)}(a,b) = \frac{K_{IC}^{(2)}}{\sqrt{\pi \mathrm{q}/2}} \sqrt{\frac{1 + 2a/\mathrm{q}(1 + 2a/b)^{-2}}{1 + 2a/\mathrm{q}}} = \sigma_{IC}^{(2)} \sqrt{\frac{1 + 2a/\mathrm{q}(1 + 2a/b)^{-2}}{1 + 2a/\mathrm{q}}} \tag{18}$$

If the half axes *a* and *b* are much greater than q, then this final expression is obtained:

$$\sigma_{IC}^{(1)}(a,b) = \frac{K_{IC}^{(2)}}{\sqrt{\pi \mathrm{q}/2}} \frac{1}{(1 + 2a/b)} = \frac{\sigma_{IC}^{(2)}}{1 + 2a/b} \tag{19}$$

3.4. FM-3: mixed crack

In FM-3 (Fig. 4c) the two aforementioned modes FM-1 and FM-2 coexist and the critical stress is assumed to be predicted by a mean field approach as:

$$\sigma_{IC}^{(M)} = \sigma_{IC}^{(12)} \cdot \frac{A_d}{\alpha A} + \sigma_{IC}^{(1)} \cdot \left(1 - \frac{A_d}{\alpha A}\right) \tag{20}$$

wherein A_d is the final delamination area (different from αA as a consequence of the intrinsic fracture on the complementary surface $\alpha A - A_d$); the superscript "*M*" denotes the mixed crack.

4. Results and discussion

4.1. Micro-structural analysis

Fig. 5a reports the XRD pattern of as-poured SCNA; the presence of a broad halo (2θ within 20-35°) without any diffractions peak, reveals the completely amorphous nature of SCNA after melting. As

shown in Fig. 5b, the thermal treatment of sintering (1000 °C for 3 h) induced the nucleation of $CaSiO_3$ (wollastonite; PDF database code 00-027-0088), known as a highly biocompatible crystalline phase [33,34]. As the thermally-treated SCNA is a glass-ceramic materials, hereafter it will be referred to as GC-SCNA.

4.2. Morphological investigations

Fig. 6a demonstrates the glass-ceramic nature of the sintered intermediate coating, as the presence of needle-shaped white crystals embedded in a dark matrix (residual glass phase) is clearly distinguishable. Fig. 6b showed that these white crystals were constituted by calcium (Ca), silicon (Si) and oxygen (O) (small amounts of Na and Al were also detected due to "boundary effects" as they were contained in the surrounding amorphous matrix; Ag is due to the thin metal coating necessary for the analysis): this observation was fully consistent with XRD results, further demonstrating the existence of $CaSiO_3$ as the unique crystalline phase. Fig. 6a also demonstrated that the interface between GC-SCNA intermediate coating and alumina was defect- and crack-free, thereby proving the suitability of SCNA as excellent material to coat alumina substrates, in good accordance with previous observations by the authors [23].

From an architectural viewpoint, the GC-SCNA scaffold closely mimicked the foam-like 3-D structure of cancellous bone (Fig. 6c). The total porosity of the scaffold (about 63 %vol.) was comparable to that of human spongy bone (typically in the 50-70 %vol. range [4]) and its highly interconnected network of macropores within 100-600 μm (Fig. 6d) is a valuable feature to allow bone cells colonization and implant vascularisation *in vivo*.

Fig. 6e reports the SEM micrograph of a polished cross-section of a complete sample showing the components of its 3-layer structure.

4.3. Model results: outcomes and potential of the QFM-based approach

The bonding strength of the GC-SCNA trabecular-like coatings to alumina flat substrate was studied by employing the model developed in the section 3.

The parameters used as model inputs were given as follows:

- layers thicknesses: $l^{(1)} = 2.0$ mm, $l^{(2)} = 0.2$ mm, $l^{(3)} = 1.0$ mm
- elastic moduli: $E^{(1)} = 20$ GPa, $E^{(2)} = 90$ GPa, $E^{(3)} = 400$ GPa
- initial bonding area, A ($A = 111.1 \pm 16.3$ mm^2 for experiment 1, whereas A was assumed to be 100.0 mm^2 for experiments 2 and 3, being the samples fabricated by using 10 × 10 mm^2 alumina plates)
- delaminating area, A_d, that was experimentally measured for each sample after the mechanical test ($A_d = 77.8 \pm 22.2$ mm^2 for experiment 2 and $A_d = 88.0 \pm 9.9$ mm^2 for experiment 3).
- failure stress, σ_t, that was experimentally measured for each sample ($\sigma_t = 3.7 \pm 1.1$ MPa for experiment 1, $\sigma_t = 20.8 \pm 1.9$ MPa for experiment 2 and $\sigma_t = 1.7 \pm 0.4$ MPa for experiment 3).

From the experimental observations, it is worth underlining that the failure in experiment 1 corresponds to FM-2 whereas the experiments 2 and 3 to FM-3 (being $A_d < A$ in all cases); FM-1 is absent in the experiments.

The elastic moduli are comparable to those assessed by other authors using acoustic methods on porous glass-ceramics with analogous porosity [18].

The fitting of the experimental data to estimate the unknown parameters of the model was carried out by using a proper code developed with MATLAB software (least mean squares algorithm).

For experiment 1, employing Eq.(19) with the assumption $a/b = k/A$ yields:

$$\sigma_{IC}^{(1)}(a,b) = \frac{\sigma_{IC}^{(2)}}{1+2k/A}$$

Data fitting (Fig. 7a) allowed to obtain $\sigma_{IC}^{(2)}$ = 47 MPa and k = 651 mm^2.

For experiment 2, mixed mode (FM-3) was observed (Fig. 4c) between GC-SCNA dense coating and alumina substrate. Applying Eq.(20) and assuming $\alpha = 1$ gives:

$$\sigma_{IC}^{(M)} = 2\sqrt{\frac{E^{(2)}E^{(3)}\frac{A_d}{A}}{l^{(2)}E^{(3)}\sqrt{\frac{A_d}{A}}+2l^{(3)}E^{(2)}}G_{IC}^{(23)}\cdot\frac{A_d}{A}} + \sigma_{IC}^{(2)}\cdot\left(1-\frac{A_d}{A}\right)$$

wherein $\sigma_{IC}^{(2)}$ = 47 MPa has already been calculated from experiment 1. By best fitting of the data (Fig. 7b), $G_{IC}^{(23)} = 0.46$ N/m was obtained.

FM-3 was also observed in experiment 3; the bonding strength, assuming $\alpha = 1$, can be predicted as:

$$\sigma_{IC}^{(12)} = 2\sqrt{\frac{E^{(1)}E^{(2)}\frac{A_d}{A}}{l^{(1)}E^{(2)}\sqrt{\frac{A_d}{A}}+2l^{(2)}E^{(1)}}G_{IC}^{(12)}\cdot\frac{A_d}{A}} + \frac{\sigma_{IC}^{(2)}}{1+2k/A}\cdot\left(1-\frac{A_d}{A}\right)$$

Likewise, by best fitting of the data (Fig. 7c) $G_{IC}^{(12)} = 0.065$ N/m was obtained.

Fitting the experimental data by the present theory showed that the scaffold strength increases as the cross-sectional area increases in the experiment 1 carried out on the GC-SCNA trabecular-like coating (scaffold) alone (Fig. 7a). Fig. 7b shows that the delaminating strength between the GC-SCNA dense intermediate coating and alumina substrate decreases as the delaminating area increases. However, in Fig. 7c, although the trend of the fitting curve is also decreasing, its slope is

close to zero, which is different from that shown in Fig. 7b; this can be explained considering (i) the small difference between the delaminating strength between GC-SCNA trabecular-like coating and GC-SCNA interlayer and the scaffold strength, and (ii) the large difference between the delaminating strength between GC-SCNA interlayer and ceramic substrate and interlayer strength.

The QFM-based model developed in the present work is useful not only to estimate important mechanical parameters, such as the fracture toughness of the material, but it can act as a valuable tool to be applied at the design stage of the desired device. Specifically, it would be very useful to investigate the influence of some key design parameters that can be properly controlled by manufacturers/researchers, such as geometry and elastic properties of the involved biomaterials, with the aim of optimizing the structural and mechanical behaviour of the system. As a representative example, the influence of two dimensionless parameters, namely l_1/l_2 and E_1/E_2, was studied in the case of the mixed mode (FM-3) by employing the fitted strain energy release rate $G_{IC}^{(12)} = 0.065\,\mathrm{N/m}$.

It is worth mentioning that, from the designer's viewpoint, it would be of utmost importance to investigate the influence of varying biomaterial porosity on the mechanical strength of the system. For instance, the processing parameters of glass-derived porous biomaterials, such as the trabecular-like coatings analyzed in the present work, can be varied in a controlled way to obtain a desired pore content which plays a key role in affecting the mechanical properties of the material [12,13,16]. The Young's modulus of a given (bio)material is known to be dependent on its pores content [18]; therefore, the analysis of the influence of the parameter E_1/E_2 on the bonding strength also allows to take into account the effect of pores content (as variations of porosity involve variations in the elastic modulus) [18]. The analytical results are reported in Fig. 8; the increase of the two

dimensionless quantities resulted in different behaviours: (1) the higher l_1/l_2 – namely the higher the thickness of trabecular-like layer –, the lower the bonding strength; (2) the higher E_1/E_2 – namely the higher the Young's modulus of trabecular-like layer –, the higher the bonding strength. From these data it is possible to conclude that the bonding behaviour of the device can be improved by reducing the scaffold thickness, or by increasing the Young's modulus of the scaffold, or else by acting simultaneously on both parameters.

The impact of the approach proposed in the present work over the biomaterials design could be very significant in the near future. Ideally, the suggested method would allow overcoming the limitations and inaccuracies of the traditional "trial and error" approach to optimize the mechanical performances of biomaterials and implants. Furthermore, unwanted losses of experimental time used for samples preparation could be successfully avoided.

4.4. Considerations on the suitability of the chosen biomaterials, limitations of the present study and future perspectives

In this work, the experimental glass SCNA was selected as starting material to produce trabecular-like coatings (scaffolds) intended to promote the osteointegration of prosthetic devices (Fig. 1). As discussed elsewhere by the authors [23], the choice of SCNA was mainly due to the need for proposing high-strength porous biomaterials able to potentially withstand the loads that physiologically act on a real hip joint prosthesis: the compressive strength of GC-SCNA scaffolds (~13 MPa [23]) was comparable and even slightly superior to that of natural cancellous bone (2-12 MPa [1]), and therefore SCNA seemed to be very suitable for the intended scope. Trabecular

coatings based on the well-known 45S5 Bioglass®, for instance, are to be considered unsuitable due to their dramatic brittleness (the literature shows that Bioglass®-derived glass-ceramic scaffolds exhibit a compressive strength lower that 1 MPa [35,36]); therefore, the search for an alternative, new and more mechanically effective biomaterial was necessary. Currently, the development of porous glass-based biomaterials with mechanical strength and architectural features comparable to those of natural cancellous bone is one of the most challenging topics of bone tissue engineering research [5-7,12,13,21,37-39].

However, as shown elsewhere by the authors [23], the major drawback of GC-SCNA is its low bioactivity. *In vitro* tests in acellular simulated body fluids (SBF) mimicking the ionic composition of human plasma are commonly recognized as a standard procedure used for estimating the bioactive potential of biomaterials. On the basis of a lot of experimental work carried out in the last thirty years [40-42], the majority of researchers currently agrees that the formation *in vitro* of a hydroxyapatite layer on the surface of biomaterials is a fundamental pre-condition to reasonably predict the *in vivo* bioactive behaviour (bone-bonding ability) of the implant. In recent years, however, the suitability of SBF has been called into question [43] and a recent work by Towler et al. [44] indicates that forecasting a material ability to bond to bone based on SBF experiments may provide a false negative result. Therefore, the apparently low *in vitro* bioactivity of GC-SCNA trabecular-like layer [23] could be enhanced in an *in vivo* environment; furthermore, the coatings could lead to osteogenesis *in vivo* by virtue of the key role played by their bone-like porous architecture [24]. In view of future research work on SCNA, surface functionalization by means of appropriate organic molecules could also contribute to improve the material bioactivity and osteointegration potential [45].

It is also interesting to underline that the mechanical properties of bioceramic scaffolds can significantly increase *in vivo* due to tissue in-growth [46]: in fact, the cells adherent on scaffold struts, the newly formed tissue and the scaffold itself create a biocomposite *in situ*, thereby increasing the time-dependent strength of the implanted construct. At present, the GC-SCNA trabecular-like coatings were mechanically tested only in "dry" conditions; it is reasonable to expect that, after implantation *in vivo*, their actual strength can become superior to that assessed before the contact with the biological environment.

The feasibility of SCNA-derived trabecular-like coatings was successfully demonstrated on flat geometry, and the bonding strength of the coating to the substrate was modelled in this work following an innovative QFM-based approach. The major goal achieved in this article was to carry a novel contribution for linking the experimental approach to the theoretical one for the development and analysis of biomaterials and implantable devices. Indeed, the majority of medical implants are characterized by complex, often curved shapes, like the semi-spherical geometry that is typical of the acetabular component of hip joint prostheses (Fig. 1); therefore, the pilot results achieved in this study will deserve an extension to a real 3-D configuration. It will be necessary to set up appropriate manufacturing technique to fabricate curved trabecular-like coatings on ceramic cups, and then an appropriate QFM-based model for this curved geometry can be developed; in such a context, optimization of scaffold shaping and coating techniques is currently in progress in the framework of an European Project (MATCh – "Monoblock Acetabular cup with Trabecular-like Coating", Grant Agreement n. 286548).

5. Conclusions

In this work, the bonding strength of glass-derived trabecular-like coatings to ceramic substrates for prosthetic applications was investigated, following a new approach based on the combination between experimental results and quantized fracture mechanics theory. It was observed that, in the considered 3-layer structure, the crack mixed mode (intrinsic fracture and interface delamination) always takes place. By fitting the experimental data with the theoretical prediction, additional mechanical properties of the system were identified, such as the fracture toughness; this parameter was then introduced into the model to further study the influence of different system parameters on the boding strength. The model and concepts reported in this paper represent a novel approach towards a more rational design of biomaterials and coatings for bone tissue engineering applications.

Acknowledgements

This work was partially funded by the EU Network of Excellence project "Knowledge-based Multicomponent Materials for Durable and Safe Performance" (KMM-NoE, NMP3-CT-2004-502243).

N.P. was supported by the European Research Council under the European Union's Seventh Framework Programme (FP7/2007-2013)/ERC Grant agreement n. 279985.

References

[1] L.L. Hench, Bioceramics: from concept to clinic, J. Am. Ceram. Soc. 74 (1991) 1487-1510.

[2] A.L. Boskey, Mineralization of bone and teeth, Elements 3 (2007) 385-391.

[3] S. Tassani, C. Ohman, M. Baleani, F. Baruffaldim M. Viceconti, Anisotropy and inhomogeneity of the trabecular structure can describe the mechanical strength of osteoarthritic cancellous bone, J. Biomech. 43 (2010) 1160-1166.

[4] V. Karageorgiou, D. Kaplan, Porosity of 3D biomaterial scaffolds and osteogenesis, Biomaterials 26 (2005) 5474-5491.

[5] J.R. Jones, E. Gentleman, J. Polak, Bioactive glass scaffolds for bone regeneration, Elements 3 (2007) 393-399.

[6] F. Baino, C. Vitale-Brovarone, Three-dimensional glass-derived scaffolds for bone tissue engineering: current trends and forecasts for the future, J. Biomed. Mater. Res. A 97 (2011) 514-535.

[7] H. Fu, Q. Fu, N. Zhou, W. Huang, M.N. Rahaman, D. Wang, X. Liu, In vitro evaluation of borate-based bioactive glass scaffolds prepared by a polymer foam replication method, Mater. Sci. Eng. C 29 (2009) 2275-2281.

[8] A. Hoppe, N.S. Guldal, A.R. Boccaccini, A review of the biological response to ionic dissolution products from bioactive glasses and glass-ceramics, Biomaterials 32 (2011) 2757-2774.

[9] L.C. Gerhardt, K.L. Widdows, M.M. Erol, C.V. Burch, J.A. Sanz-Herrera, I. Ochoa, R. Stampfli, I.S. Roqan, S. Gabe, T. Ansari, A.R. Boccaccini, The pro-angiogenic properties of multi-functional bioactive glass composite scaffolds, Biomaterials 32 (2011) 4096-4108.

[10] S.J. Hollister, Porous scaffold design for tissue engineering, Nat. Mater. 4 (2005) 518-524.

[11] K. Rezwan, Q.Z. Chen, J.J. Blaker, A.R. Boccaccini, Biodegradable and bioactive porous polymer/inorganic composite scaffolds for bone tissue engineering, Biomaterials 27 (2006) 3413-3431.

[12] C. Vitale-Brovarone, F. Baino, E. Verné, High strength bioactive glass-ceramic scaffolds for bone regeneration, J. Mater. Sci. Mater. Med. 20 (2009) 643-653.

[13] F. Baino, M. Ferraris, O. Bretcanu, E. Verné, C. Vitale-Brovarone, Optimization of composition, structure and mechanical strength of bioactive 3-D glass-ceramic scaffolds for bone substitution, J. Biomater. Appl. (in press) DOI: 10.1177/0885328211429193

[14] C. Vitale-Brovarone, F. Baino, E. Verné, Feasibility and tailoring of bioactive glass-ceramic scaffolds with gradient of porosity for bone grafting, J. Biomater. Appl. 24 (2010) 693-712.

[15] L.C. Gerhardt, A.R. Boccaccini, Bioactive glass and glass-ceramic scaffolds for bone tissue engineering, Materials 3 (2010) 3867-3910.

[16] F. Baino, E. Verné, C. Vitale-Brovarone, 3-D high strength glass-ceramic scaffolds containing fluoroapatite for load-bearing bone portions replacement, Mater. Sci. Eng. C 29 (2009) 2055-2062

[17] A. Fritsch, L. Dormieux, C. Hellmich, J. Sanahuja, Mechanical behavior of hydroxyapatite biomaterials: an experimentally validated micromechanical model for elasticity and strength, J. Biomed. Mater Res. A 88 (2007) 149-161.

[18] A. Malasoma, A. Fritsch, C. Kohlhauser, T. Brynk, C. Vitale-Brovarone, Z. Pakiela, J. Eberhardsteiner, C. Hellmich, Micromechanics of bioresorbable porous CEL2 glass ceramic scaffolds for bone tissue engineering, Adv. Appl. Ceram. 107 (2008) 277-286.

[19] S. Scheiner, R. Sinibaldi, B. Pichler, V. Komlev, C. Renghini, C. Vitale-Brovarone, F. Rustichelli, C. Hellmich, Micromechanics of bone tissue-engineering scaffolds, based on resolution error-cleared computer tomography, Biomaterials 30 (2009) 2411-2419.

[20] M.N. Rahaman, D.E. Day, B.S. Bal, Q. Fu, S.B. Jung, L.F. Bonewald, A.P. Tomsia, Bioactive glass in tissue engineering, Acta Biomater. 7 (2011) 2355-2373.

[21] Q. Fu, E. Saiz, M.N. Rahaman, A.P. Tomsia, Bioactive glass scaffolds for bone tissue engineering: state of the art and future perspectives, Mater. Sci. Eng. C 31 (2011) 1245-1256.

[22] E. Verné, C. Vitale-Brovarone, L. Robiglio, F. Baino, Single-piece ceramic prosthesis elements, Patent WO 2008/146322 A2 (2008).

[23] C. Vitale-Brovarone, F. Baino, F. Tallia, C. Gervasio, E. Verné, Bioactive glass-derived trabecular coating: a smart solution for enhancing osteointegration of prosthetic elements, J. Mater Sci. Mater. Med. 23 (2012) 2369-2380.

[24] N. Pugno, R. Ruoff, Quantized fracture mechanics, Phil. Mag. 84 (2004) 2829-2845.

[25] N. Pugno, Dynamic quantized fracture mechanics, Int. J. Fract. 140 (2006) 159-168.

[26] N. Pugno, New quantized failure criteria: application to nanotubes and nanowires, Int. J. Fracture 141 (2006) 311-323.

[27] J.E. Ritter, D.C. Greenspan, R.A. Palmer, L.L. Hench, Use of fracture mechanics theory in lifetime predictions for alumina and bioglass-coated alumina, J. Biomed. Mater. Res. A 13 (1979) 251-263.

[28] H.M. Kim, F. Miyaji, T. Kokubo, T. Nakamura, Bonding strength of bonelike apatite layer to Ti metal substrate, J. Biomed. Mater. Res. A 38 (1997) 121-127.

[29] X. Zheng, M. Huang, C. Ding C, Bond strength of plasma-sprayed hydroxyapatite/Ti

composite coatings, Biomaterials 21 (2000) 841-849.

[30] M.H. Hong, D.H. Lee, K.M. Kim, Y.K. Lee, Improved bonding strength between TiO_2 film and Ti substrate by microarc oxidation, Surf. Interface Anal. 42 (2010) 492-496.

[31] ASTM F1538-03 (2009), Standard specification for glass and glass ceramic biomaterials for implantation

[32] ASTM C633-01 (2008), Standard test method for adhesion or cohesion strength of thermal spray coatings.

[33] T. Kokubo, S. Ito, S. Sakka, T. Yamamuro, Formation of a high-strength bioactive glass-ceramic in the system MgO-CaO-SiO_2-P_2O_5, J. Mater. Sci. 21 (1986) 536-540.

[34] W. Xue, X. Liu, X.B. Zheng, C. Ding C, In vivo evaluation of plasma-sprayed wollastonite coating, Biomaterials 26 (2005) 3455-3460.

[35] Q.Z. Chen, I.D. Thompson, A.R. Boccaccini, 45S5 Bioglass®-derived glass-ceramic scaffolds for bone tissue engineering, Biomaterials 27 (2006) 2414-2425.

[36] O. Bretcanu, Q. Chen, S.K. Misra, A.R. Boccaccini, E. Verné, C. Vitale-Brovarone, Biodegradable polymer coated 45S5 Bioglass-derived glass-ceramic scaffolds for bone tissue engineering, Glass Tech. Eur. J.: Glass Sci. Tech. A 48 (2007) 227-234.

[37] C. Vitale-Brovarone, F. Baino, M. Miola, R. Mortera, B. Onida, E. Verné, Glass-ceramic scaffolds containing silica mesophases for bone grafting and drug delivery, J. Mater. Sci. Mater. Med. 20 (2009) 809-820.

[38] C. Vitale-Brovarone, F. Baino, O. Bretcanu, E. Verné, Foam-like scaffolds for bone tissue engineering based on a novel couple of silicate-phosphate specular glasses: synthesis and properties, J. Mater. Sci. Mater. Med. 20 (2009) 2197-2205.

[39] C. Renghini, A. Giuliani, S. Mazzoni, F. Brun, E. Larsson, F. Baino, C. Vitale-Brovarone. Microstructural characterization and in vitro bioactivity of porous glass-ceramic scaffolds for bone regeneration by synchrotron radiation X-ray microtomography, J. Eur. Ceram. Soc. (in press) DOI: 10.1016/j.jeurceramsoc.2012.10.016

[40] O.H. Andersson, G. Liu, K.H. Karlsson, J. Juhanoja, In vivo behaviour of glasses in the SiO_2-Na_2O-CaO-P_2O_5-Al_2O_3-B_2O_3 system, J. Mater. Sci.: Mater. Med. 1 (1990) 219-227.

[41] T. Kokubo, H. Takadama, How useful is SBF in predicting in vivo bone bioactivity?, Biomaterials 27 (2006) 2907-2915.

[42] L.L. Hench, The story of Bioglass®, J. Mater. Sci.: Mater. Med. 17 (2006) 967-978.

[43] M. Bohner, J. Lemaitre, Can bioactivity be tested in vitro with SBF solution?, Biomaterials 20 (2009) 2175-2179.

[44] M.R. Towler, D. Boyd, C. Freeman, I.M. Brook, P. Farthing, Comparison of in vitro and in vivo bioactivity of SrO-CaO-ZnO-SiO_2 glass grafts, J. Biomater. Appl. 23 (2009) 561-572.

[45] E. Verné, S. Ferraris, C. Vitale-Brovarone, S. Spriano, C.L. Bianchi, A. Naldoni, M. Morra, C. Cassinelli, Alkaline phosphatase grafting on bioactive glasses and glass-ceramics, Acta Biomater, 6 (2010) 229-240.

[46] N. Tamai, A. Myoui, T. Tomita, T. Nakase, J. Tanaka, T. Ochi, Novel hydroxyapatite ceramics with an interconnective porous structure inhibit superior osteoconduction in vivo, J. Biomed. Mater. Res. 59 (2002) 110-117.

Figure

Fig. 1. Scheme of the innovative acetabular cup disclosed in the patent [22] deposited by the authors; this monoblock ceramic implant is constituted by three elements: (i) a bioinert ceramic substrate, that articulates directly with the (prosthetic) femur head; (ii) a bioactive trabecular coating, i.e. a glass-derived scaffold, that aims at promoting implant osteointegration to patient's pelvis bone; (iii) a glass-derived (pore-free or minimally porous) interlayer, able to improve the adhesion between alumina substrate (cup) and trabecular coating (scaffold). (Figure reproduced from Vitale-Brovarone et al. [23] with permission by Springer).

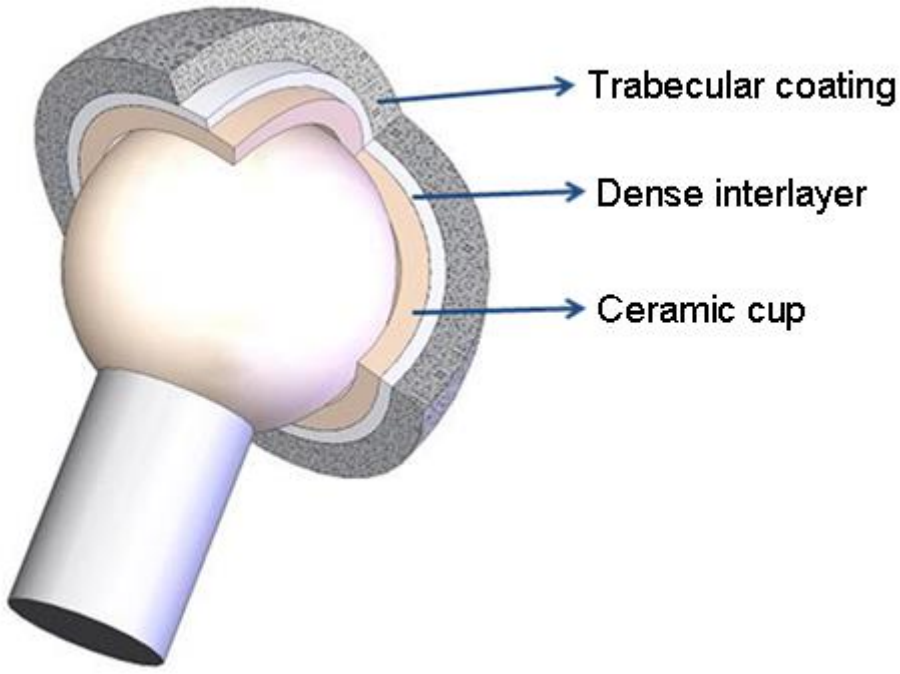

Fig. 2. Processing stages (1-5) involved in samples preparation.

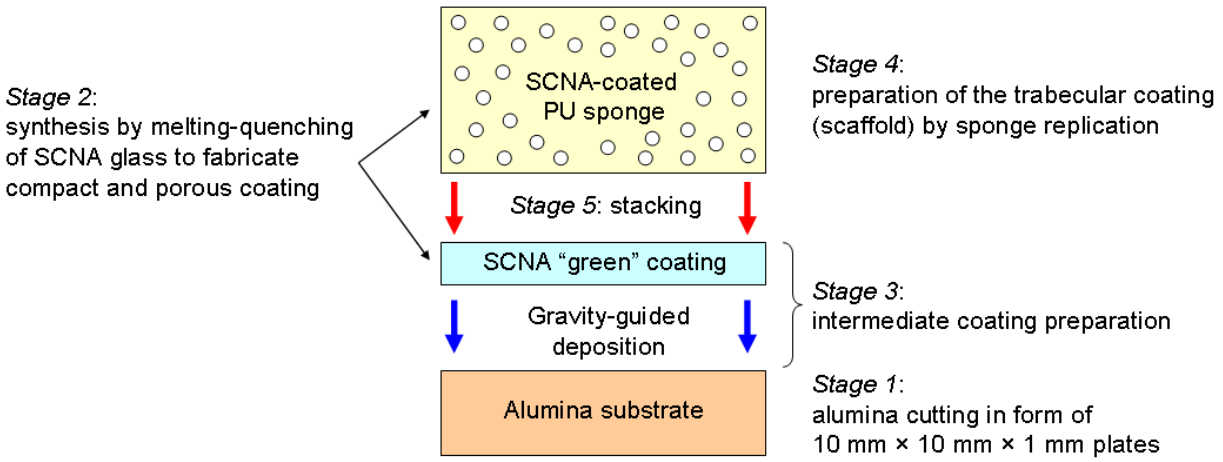

Fig. 3. Scheme of the device: (a) parts and nomenclature; (b) cracking mechanism; (c) top view after failure.

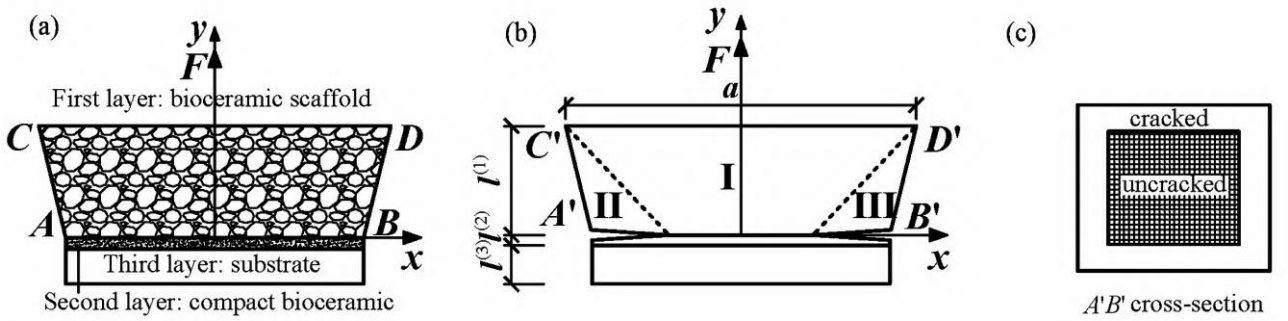

Fig. 4. Failure modes: (a) mode 1 (delamination at the substrate/intermediate layer interface); (b) mode 2 (failure in the scaffold); (c) mode 3 (mixed failure).

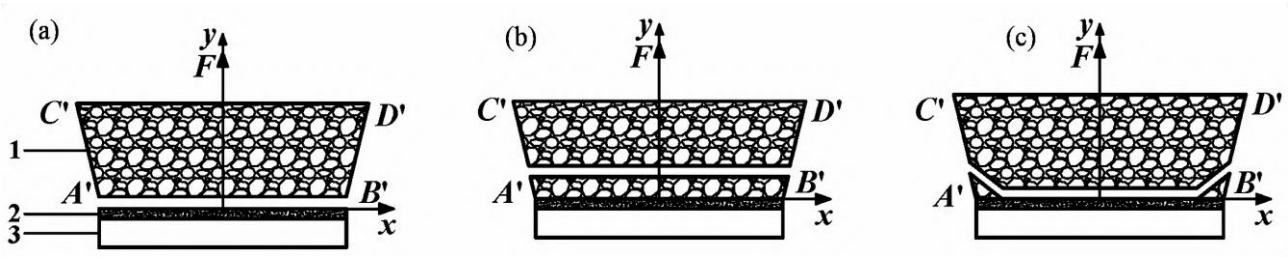

Fig. 5. XRD patterns of (a) as-melt SCNA and (b) thermally-treated SCNA (sintering at 1000 °C for 3 h).

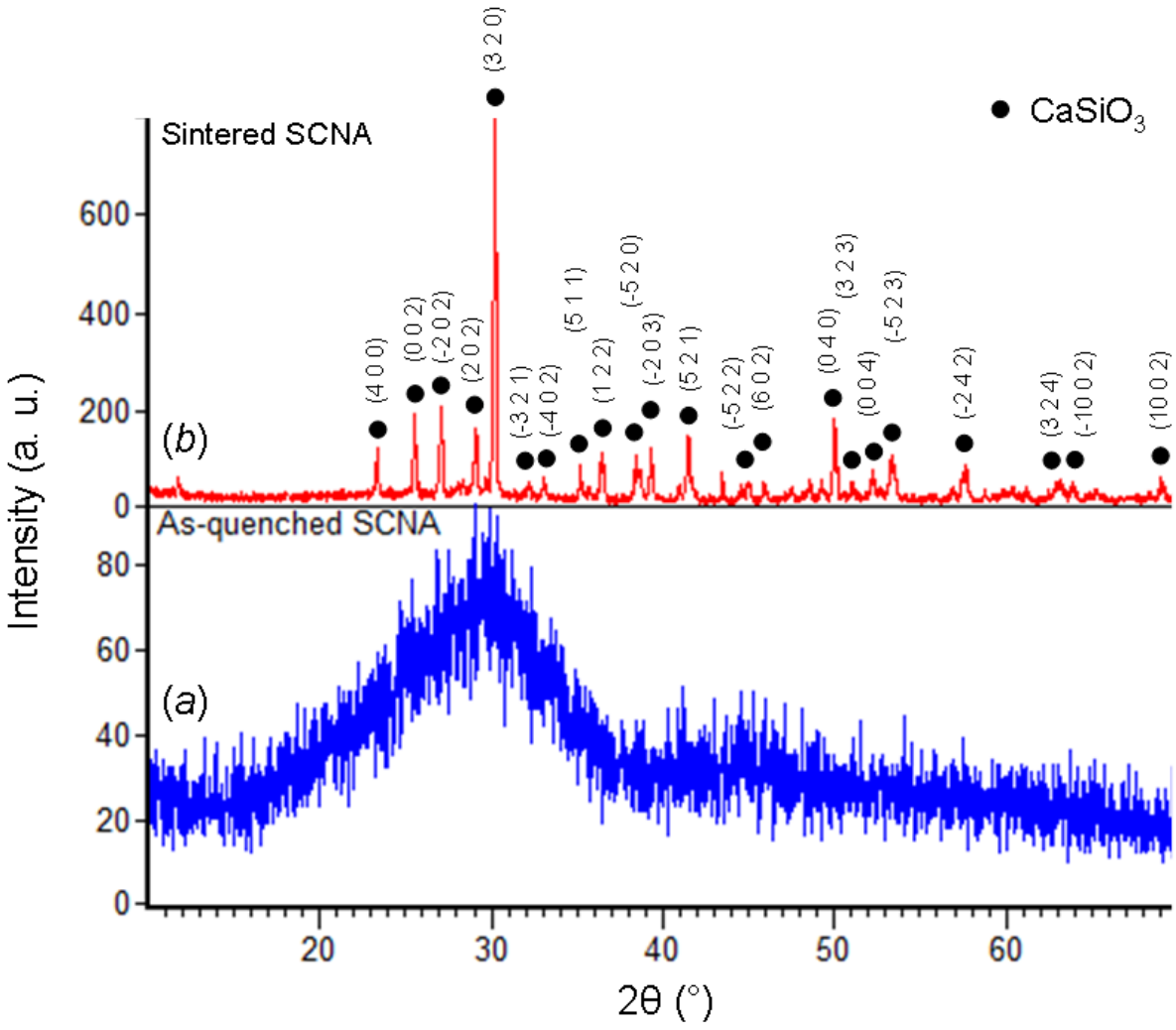

Fig. 6. Samples analysis by SEM-EDS: (a) GC-SCNA intermediate coating (SEM back-scattering mode); (b) EDS analysis of the needle-shaped white crystals observed in (a); (c) GC-SCNA scaffold surface (top view); (d) GC-SCNA scaffold cross-section; (e) cross-section (SEM back-scattering mode) of the complete 3-layer sample (alumina substrate + dense interlayer + trabecular-like coating).

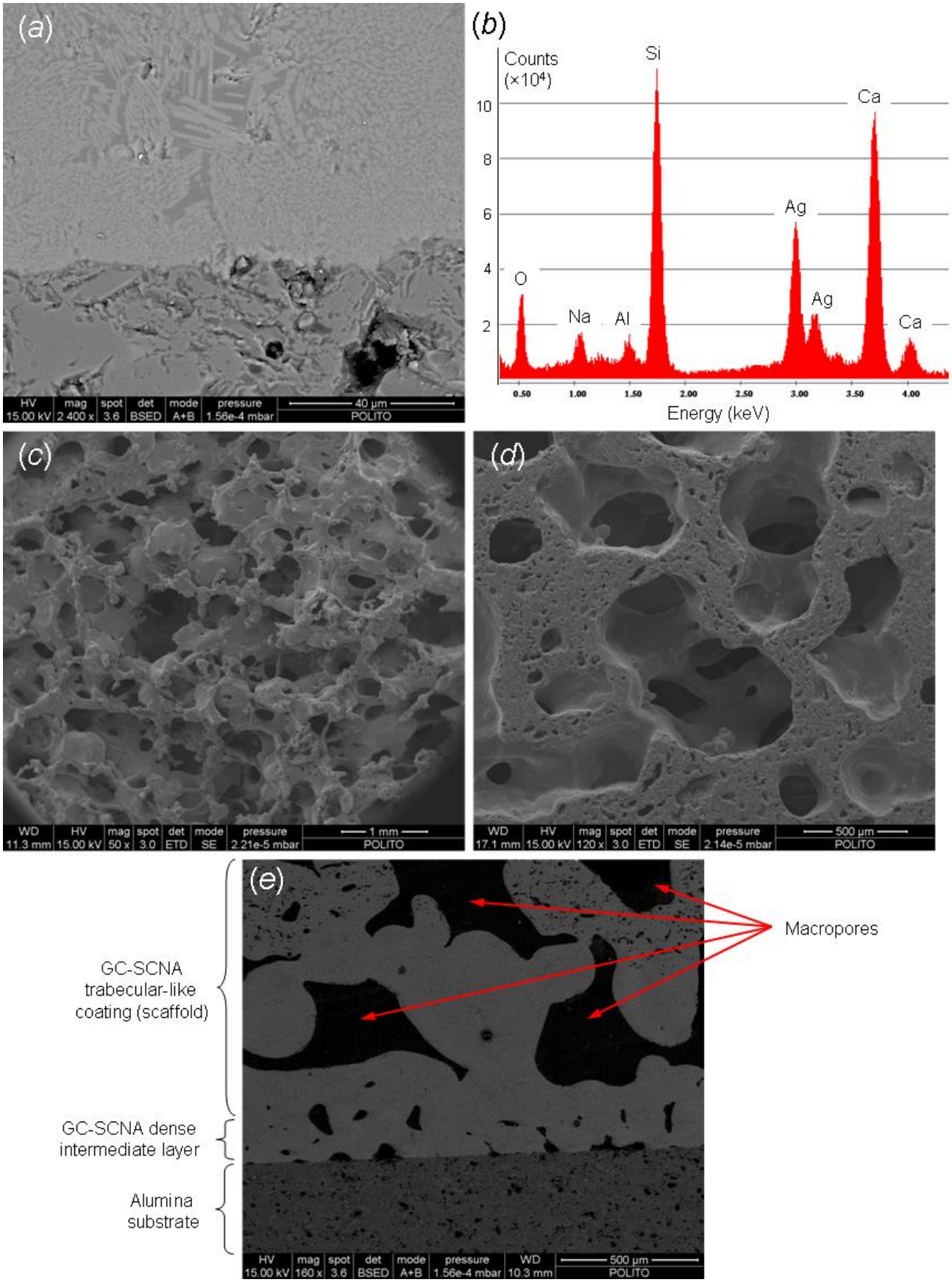
(a)
HV 15.00 kV | mag 2 400 x | spot 3.6 | det BSED | mode A+B | pressure 1.56e-4 mbar | 40 µm | POLITO
(b)
Counts (×10⁴)
10
8
6
4
2
Si
Ca
Ag
Ag
O
Na
Al
Ca
0.50
1.00
1.50
2.00
2.50
3.00
3.50
4.00
Energy (keV)
(c)
WD 11.3 mm | HV 15.00 kV | mag 50 x | spot 3.0 | det ETD | mode SE | pressure 2.21e-5 mbar | 1 mm | POLITO
(d)
WD 17.1 mm | HV 15.00 kV | mag 120 x | spot 3.0 | det ETD | mode SE | pressure 2.14e-5 mbar | 500 µm | POLITO
(e)
GC-SCNA trabecular-like coating (scaffold)
GC-SCNA dense intermediate layer
Alumina substrate
Macropores
HV 15.00 kV | mag 160 x | spot 3.6 | det BSED | mode A+B | pressure 1.56e-4 mbar | WD 10.3 mm | 500 µm | POLITO

Fig. 7. Comparison between experimental results and theoretical predictions (a) experiment 1, (b) experiment 2 and (c) experiment 3.

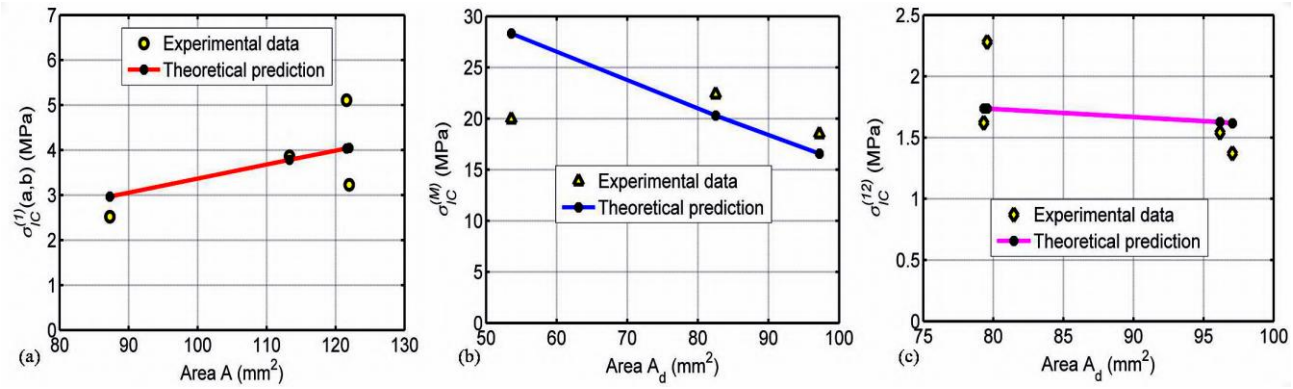

Fig. 8. The potential of the QFM-based approach: an example on how to use the developed model to predict the bonding strength of the trabecular coating in a flat configuration in order to optimize the device mechanical properties. Variation of the model parameters: in the influence of l_1/l_2, l_1 varies from 0.2 mm to 2.0 mm; in the influence of E_1/E_2, E_1 varies between 9 GPa to 90 GPa; in both cases, E_2 = 90 GPa, l_2 = 0.2 mm, α = 1.0, $G_{IC}^{(12)} = 0.065$ N/m, A_d = 88.0 mm^2.

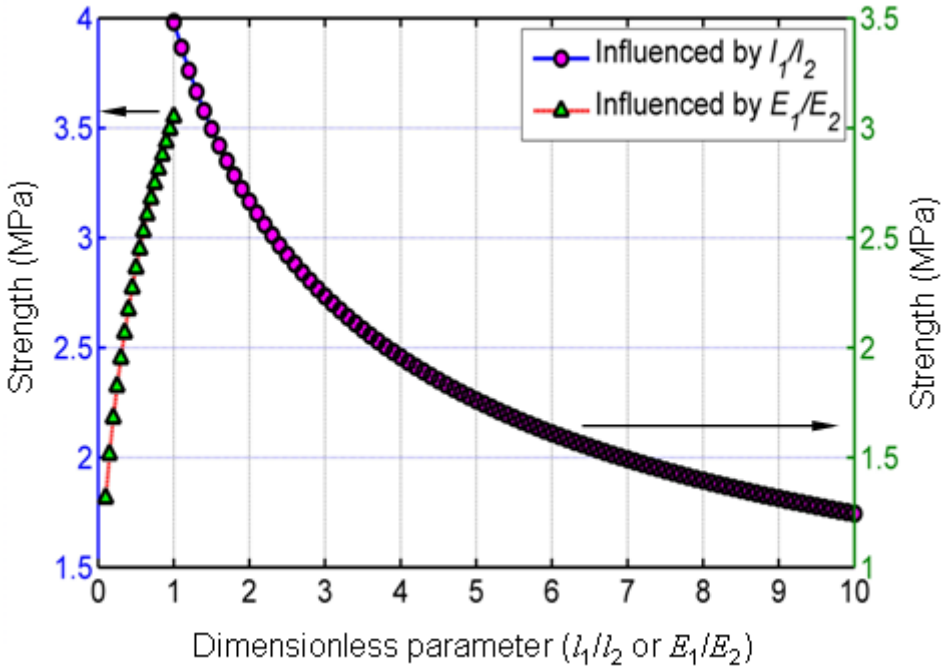

.

Tables

Table 1. Cycle of fabrication of the sample investigated in this work.

Stage	Description
1	High-purity alumina (> 99.5%) 1-mm thick sheets (Goodfellow, Cambridge, UK) were cut by means of a rotating diamond wheel (Accutom 5 Machine, Struers) to obtain squared 10 mm × 10 mm plates.
2	A silicate glass (SCNA; molar composition: $57SiO_2$-$34CaO$-$6Na_2O$-$3Al_2O_3$) was prepared by melting the raw products (SiO_2, purity 99.0%, Sigma-Aldrich; $CaCO_3$, purity 99.0%, Sigma-Aldrich; Na_2CO_3, purity 99.5%, Sigma-Aldrich; Al_2O_3, purity 99.9%, Alfa-Aesar) in a platinum crucible at 1500 °C for 1 h in air and then by quenching the melt in cold water to obtain a "frit", that was subsequently ground by a 6-balls zirconia milling and eventually sieved to obtain glass particles below 32 μm.
3	SCNA "green" coatings on the alumina plates were prepared by gravity-guided deposition after suspending a proper amount of glass particles (0.7 g) in ethanol (beaker diameter: 56 mm) to finally obtain a 100-μm thick layer
4	Commercial open-cells polyurethane sponge (apparent density ~20 kg m^{-3}) was cut in 4-mm thick blocks to be impregnated with a water-based SCNA-containing slurry (the glass particles were prepared at the end of Stage 2), according to an optimized schedule proposed for sponge replication method [12].
5	SCNA-impregnated sponge (prepared in Stage 4) was stacked on the "green" SCNA coating (prepared in Stage 3).
6	The whole system was thermally treated in air at 1000 °C for 3 h (heating rate 5 °C min^{-1}; cooling rate 10 °C min^{-1}) to allow the burning-out of the polymer template and the glass powders sintering.